Available online at www.sciencedirect.com

ScienceDirect

IFAC PapersOnline CONFERENCE PAPER ARCHIVE

IFAC PapersOnLine 59-5 (2025) 73–78

Health-conscious MPC for PEM fuel cells considering main degradation mechanisms of cathode catalyst

Johanna Bartlechner * **Christoph Hametner** *
Stefan Jakubek *
* *TU Wien, Institute of Mechanics and Mechatronics, Getreidemarkt 9, Vienna, 1060, Austria*

Abstract:
The integration of fuel cell systems into hybrid electric vehicles presents unique challenges due to the highly dynamic power trajectories typical of automotive applications. The dynamic operation of fuel cells leads to performance degradation limiting the lifetime of fuel cells. This paper proposes a model predictive control strategy that optimizes the balance between fuel cell longevity, efficiency, and performance on the system level by adapting current, hydrogen flow, airflow, and the dew points at the inlet of the electrodes. Using a non-linear, physically motivated model that incorporates the key degradation mechanisms of the cathode catalyst layer, this approach provides a framework to optimize the operating strategy of the fuel cell system. By leveraging the information from the physical model, the controller can make health-conscious control decisions outperforming traditional and rule-based strategies.

Copyright © 2025 The Authors. This is an open access article under the CC BY-NC-ND license (https://creativecommons.org/licenses/by-nc-nd/4.0/)

Keywords: Fuel cells for Automotive Applications, Non-linear and optimal automotive control, Model predictive control, Degradation avoidance, PEM fuel cell degradation

1. INTRODUCTION

Fuel cells are a promising candidate for green mobility due to their high efficiency, fast refueling, and low emissions, making them particularly attractive for hybrid electric vehicles in the transition toward sustainable transportation. However, one major challenge remaining in deploying fuel cells for automotive applications is managing their durability, as the highly dynamic operating conditions inherent in vehicular use induce and accelerate degradation. These conditions, characterized by frequent power demand fluctuations and changes in operating points, age the fuel cell components, particularly impacting catalyst and membrane durability (Wallnöfer-Ogris et al., 2024).

In hybrid electric vehicles, the energy management system (EMS) determines the optimal power split between the fuel cell and the battery, shaping the power trajectories and ensuring that the energy demands of the system are met (Li et al., 2012). The required fuel cell power trajectory is then forwarded to the system level, where additional control objectives come into play, including the regulation of hydrogen and air flow rates and humidification within the fuel cell. These inputs must be carefully managed to maintain the necessary conditions for efficient power generation and to mitigate degradation (Daud et al., 2017).

Traditional control approaches for fuel cell systems, such as rule-based or PID control strategies, provide effective regulation of basic parameters under steady or moderately dynamic conditions. However, they lack the adaptability to handle the complex interplay between power demand and degradation seen in highly dynamic applications (Wu et al., 2020). Such conventional methods typically address either efficiency or degradation but struggle to achieve an optimal balance, highlighting the need for advanced control methodologies capable of integrating multiple objectives within a unified framework (Ghasemi et al., 2023).

To tackle this challenge, a health-conscious model predictive controller (MPC) is introduced. The controller uses a physically-motivated zero-dimensional fuel cell model including the key degradation mechanisms of the cathode catalyst layer. Due to the lumped formulation, the model provides the computational efficiency to realize long prediction horizons while also being real-time capable. Furthermore, the physical formulation enables an intuitive weighting between performance, efficiency, and longevity of the system. The paper is structured as follows: In Section 2, the needed methodology, namely the MPC formulation and the model, are described. The results are shown and discussed in Section 3. Finally, a conclusion and outlook are given in Section 4.

2. METHODOLOGY OF HEALTH-CONSCIOUS MPC

In a hybrid fuel cell vehicle, the EMS calculates the optimal power split between the fuel cell and the battery (Fig. 1). The power demand is then forwarded to the subsystems where further control objectives come into play. Besides providing power, the internal control of the fuel cell system (Fig. 1, green area) adapts additional inputs, including hydrogen and oxygen flow, pressure levels, humidity, and temperature. To enable this, a model predictive control algorithm is introduced. Using a physically

2405-8963 Copyright © 2025 The Authors. This is an open access article under the CC BY-NC-ND license.
Peer review under responsibility of International Federation of Automatic Control.
10.1016/j.ifacol.2025.07.084

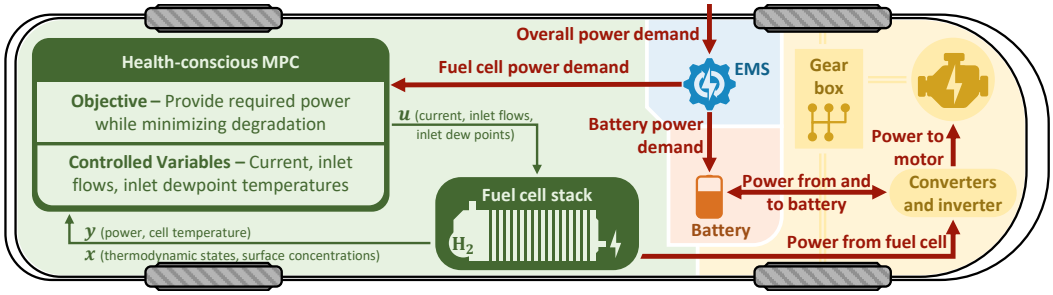

Fig. 1. **Power flow and control scheme of fuel cell hybrid vehicles including the introduced MPC.** The total power demand is provided to the energy management system (EMS) (blue), which calculates the optimal power split between the battery (red) and the fuel cell system (green). These components work together to supply the required power to the engine and the electric axle (yellow). To effectively manage the fuel cell stack, its internal control system must consider three key factors: power demand, efficiency, and lifetime. The multivariable problem is solved in real-time with the introduced health-conscious model predictive controller (MPC), which proactively adapts the system to realize anticipated power demands and enables a balanced and intuitive trade-off between performance and longevity.

motivated fuel cell model including the main degradation mechanisms on the cathode catalyst, the controller can make health-conscious decisions while also considering power requirements and cost efficiency. In this section, the needed methodology for the health-conscious controller is given, i.e., the physically motivated model is described, the MPC formulation and cost function are defined, and three aggregated key performance indices (KPI) to evaluate performance, hydrogen usage, and degradation are derived.

2.1 Real-time capable fuel cell model

A physically-motivated zero-dimensional model based on Bartlechner et al. (2024) is adapted and extended to include the main degradation mechanisms of the cathode catalyst as well as the temperature dynamics. The zero-dimensional formulation of the model assumes homogenous concentrations of the reactants in the electrode and thus does not provide any information about local phenomena or spatial distribution. However, it is computationally efficient and facilitates real-time applicability. Furthermore, the physical formulation provides insightful information about the processes within the cell. The model is continuously differentiable enabling fast linearization of the fuel cell model by the use of Jacobians. Thus providing a suitable trade-off between accuracy, predictive capacity due to physical formulation and computational efficiency.

The model in Bartlechner et al. (2024), consisting of four submodels (cathode, anode, membrane, and electrochemistry), is extended to include three additional submodels - namely, the submodel for the temperature dynamics, for electrochemical carbon corrosion, and for platinum degradation on the cathode side. The submodels are depicted in Fig. 2. Furthermore the electrochemical model is extended to include the effects of changing cell temperature on voltage, and the amount of reactants in the electrodes is formulated in terms of the amount of substance to reduce conversion efforts.

The non-linear zero-dimensional fuel cell model can be written in the input-output form

$$\dot{\mathbf{x}} = \mathbf{f}(\mathbf{x}, \mathbf{u}, \boldsymbol{\theta}), \quad \mathbf{y} = \mathbf{g}(\mathbf{x}, \mathbf{u}, \boldsymbol{\theta}) \tag{1}$$

with the state vector $\mathbf{x}$, the input vector $\mathbf{u}$, the output vector $\mathbf{y}$, the parameter vector $\boldsymbol{\theta}$, the state function vector $\mathbf{f}$ and the output function vector $\mathbf{g}$. The state vector has 25 states, and is defined as

$$\begin{aligned}\mathbf{x} =[&n_{\mathrm{O_2,ca}}, n_{\mathrm{N_2,ca}}, n_{\mathrm{H_2O_{(gas)},ca}}, n_{\mathrm{H_2O_{(liq)},ca}}, \dots \\ &n_{\mathrm{H_2,an}}, n_{\mathrm{N_2,an}}, n_{\mathrm{H_2O_{(gas)},an}}, n_{\mathrm{H_2O_{(liq)},an}}, \dots \\ &a_{\mathrm{M}}, T, \theta_{\mathrm{C^*}}, \theta_{\mathrm{C\text{-}OH}}, \theta_{\mathrm{Pt^*}}, \theta_{\mathrm{Pt\text{-}OH}}, c_{\mathrm{Pt^{2+}}}, \dots \\ &N_1, N_2, N_3, N_4, N_5, N_6, N_7, N_8, N_9, N_{10}]^{\mathrm{T}}\end{aligned} \tag{2}$$

with the amount of substance $n_{i,j}$ of the species $i \in \{\mathrm{O_2}, \mathrm{N_2}, \mathrm{H_2O_{(gas)}}, \mathrm{H_2O_{(liq)}}, \mathrm{H_2}\}$ in the electrodes $j \in \{\mathrm{ca}, \mathrm{an}\}$, the membrane humidity a_{M}, the cell temperature T, the surface concentration θ_k of $k \in \{\mathrm{C^*}, \mathrm{C\text{-}OH}, \mathrm{Pt^*}, \mathrm{Pt\text{-}OH}\}$, the $\mathrm{Pt^{2+}}$ concentration in the ionomer $c_{\mathrm{Pt^{2+}}}$, and the amount of particles N_l in the platinum particle classes $l \in \{1, 2, ..., 10\}$. The input vector consists of twelve inputs:

$$\begin{aligned}\mathbf{u} =[&\dot{n}_{\mathrm{ca,dry}}, \dot{n}_{\mathrm{an,dry}}, T_{\mathrm{dew,ca}}, T_{\mathrm{dew,an}}, p_{\mathrm{in,ca}}, p_{\mathrm{in,an}}, \dots \\ &p_{\mathrm{out,ca}}, p_{\mathrm{out,an}}, T_{\mathrm{in,ca}}, T_{\mathrm{in,an}}, T_{\mathrm{outside}}, I_{\mathrm{cell}}]^{\mathrm{T}}\end{aligned} \tag{3}$$

with the dry mole flows $n_{j,\mathrm{dry}}$, the dew point temperatures $T_{\mathrm{dew},j}$, the inlet $p_{\mathrm{in},j}$ and outlet $p_{\mathrm{out},j}$ pressures, the inlet temperatures $T_{\mathrm{in},j}$ in the electrodes $j \in \{\mathrm{ca}, \mathrm{an}\}$, the outside temperature T_{outside} and the cell current I_{cell}. The model output vector is defined as

$$\mathbf{y} = [P, T, r_{\mathrm{CO_2}}, \mathrm{ECSA}]^{\mathrm{T}} \tag{4}$$

with the cell power P, the cell temperature T, the $\mathrm{CO_2}$ formation rate $r_{\mathrm{CO_2}}$ and the electrochemical active surface area ECSA, whereby the ECSA is defined as the ratio of platinum surface to platinum mass

$$\mathrm{ECSA} = \frac{A_{\mathrm{Pt}}}{m_{\mathrm{Pt}}} = \frac{4\pi \sum_{i=1}^{10} N_i r_i^2}{\frac{4\pi}{3}\rho_{\mathrm{Pt}} \sum_{i=1}^{10} N_i r_i^3}. \tag{5}$$

Furthermore, degradation is considered by the rates of degradation

$$\mathbf{r} =[r_{\mathrm{CO_2}}, \dot{N}_1, \dot{N}_2, ..., \dot{N}_{10}]^{\mathrm{T}}. \tag{6}$$

Cathode, anode, membrane and electrochemical submodels (Fig. 2, top). The cathode and anode submodels are derived from the substance quantity balance

$$\frac{dn_{i,j}}{dt} = \dot{n}_{i,j,\mathrm{in}} - \dot{n}_{i,j,\mathrm{out}} + \dot{n}_{i,\mathrm{M}} + \dot{n}_{i,j,\mathrm{R}} \tag{7}$$

around the electrodes for the species i in the electrodes j, whereby the flows in $\dot{n}_{i,j,\mathrm{in}}$ and out $\dot{n}_{i,j,\mathrm{out}}$ of the gas

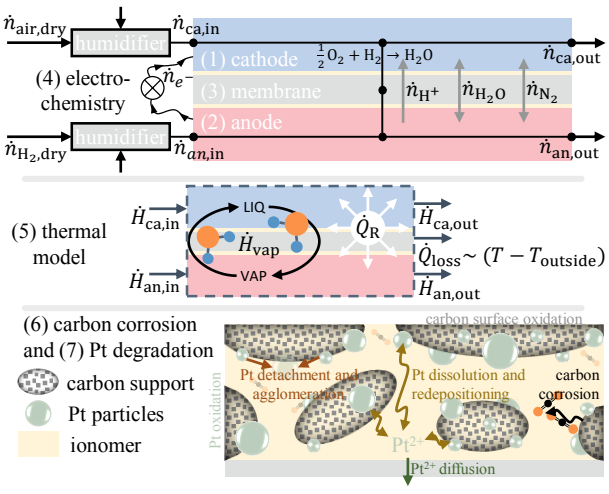

Fig. 2. **Schematics of physically motivated fuel cell model**. The (1) cathode and (2) anode submodels are derived from a material balance around the electrodes. From the (3) membrane submodel the membrane humidity is obtained. The (4) electrochemical submodel describes the effects of operating conditions on the cell voltage. The dynamics of the fuel cell temperature are obtained by the (5) thermal model. The degradation of the fuel cell is described by the submodels for (6) carbon corrosion and (7) cathode platinum degradation.

channels and the transport through the membrane $\dot{n}_{i,\mathrm{M}}$ are considered. Electrochemical reaction and phase change are combined in the reaction term $\dot{n}_{i,j,\mathrm{R}}$. The gases in the electrodes are assumed to have ideal gas behavior and are homogenously mixed within the electrodes. Water phase change is considered based on the saturation pressure at the current cell temperature. Water transport via the membrane by electroosmotic drag and back-diffusion, as well as nitrogen diffusion, is included. The membrane humidity

$$\frac{da_{\mathrm{M}}}{dt} = \frac{1}{\tau_{\mathrm{M}}}\left(\frac{a_{\mathrm{ca}} + a_{\mathrm{an}}}{2} - a_{\mathrm{M}}\right) \tag{8}$$

is derived from the humidities a_j on the anode and cathode side considering a first-order time delay. The electrochemical model is based on Kravos et al. (2020), whereby the non-isothermal formulation is used to include the effects of changing temperature on the cell voltage.

Thermal submodel (Fig. 2, middle). The dynamics of the cell temperature are obtained by an energy balance around the cell

$$\frac{dT}{dt} = \frac{1}{c_P}(\dot{H}_{\mathrm{in}} - \dot{H}_{\mathrm{out}} + \dot{H}_{\mathrm{vap}} + \dot{Q}_{\mathrm{R}} + \dot{Q}_{\mathrm{loss}}). \tag{9}$$

with the fitting parameter c_P. The convective heat flows into $\dot{H}_{\mathrm{in}}$ and out $\dot{H}_{\mathrm{out}}$ of the electrodes, the temperature changes due to the phase change of water $\dot{H}_{\mathrm{vap}}$, the generated heat $\dot{Q}_{\mathrm{R}}$ due to voltage losses as well as the conductive heat loss $\dot{Q}_{\mathrm{loss}}$ to the environment are considered.

Submodel for cathode carbon corrosion and platinum degradation (Fig. 2, bottom). A simplified model for carbon corrosion and cathode platinum degradation is derived from Pandy et al. (2013), Schneider et al. (2019), Kregar et al. (2020) and Kregar et al. (2021). The model considers carbon support surface oxidation, platinum particle surface oxidation, electrochemical carbon corrosion, Pt particle detachment and agglomeration, Pt dissolution and redeposition as well as Pt diffusion into the membrane. In comparison to Kregar et al. (2020), the Kelvin shift is averaged based on the particle distribution for the reactions changing the platinum particle surface concentration, significantly reducing the number of states.

Platinum and carbon surface oxidation, CO_2 formation and dissolution of Pt^{2+} ions are described via the reactions

$$\begin{aligned}
&\mathrm{C^*+H_2O \rightleftharpoons C\text{-}OH+H^+ + e^-} && \mathrm{E_1 = 0.20\ V\ RHE}\\
&\mathrm{C\text{-}OH \rightleftharpoons C{=}O + H^+ + e^-} && \mathrm{E_2 = 0.80\ V\ RHE}\\
&\mathrm{C^*\text{-}C\text{-}OH + H_2O \rightarrow C^* + CO_2 + 3H^+ + 3e^-} && \mathrm{E_3 = 0.95\ V\ RHE}\\
&\mathrm{Pt^* + H_2O \rightleftharpoons Pt\text{-}OH + H^+ + e^-} && \mathrm{E_4 = 0.70\ V\ RHE}\\
&\mathrm{Pt\text{-}OH \rightleftharpoons Pt{=}O + H^+ + e^-} && \mathrm{E_5 = 0.80\ V\ RHE}\\
&\mathrm{Pt\text{-}OH + C^*\text{-}C\text{-}OH \rightarrow C^* + Pt^* + CO_2 + 2H^+ + 2e^-} && \mathrm{E_6 = 0.65\ V\ RHE}\\
&\mathrm{Pt^* \rightleftharpoons Pt^{2+} + 2e^-} && \mathrm{E_6 = 1.188\ V\ RHE}
\end{aligned} \tag{10}$$

according to Pandy et al. (2013). The distribution of platinum particles is described by ten particle classes, whereby the change of particles in each class

$$\frac{dN_i}{dt} = \dot{N}_i = \dot{N}_{\mathrm{diss},i} + \underbrace{\dot{N}_{\mathrm{det},i} + \dot{N}_{\mathrm{att},i} + \dot{N}_{\mathrm{mer},i}}_{\dot{N}_{\mathrm{agg},i}} \tag{11}$$

considers particle dissolution ($\dot{N}_{\mathrm{diss},i}$) due to Ostwald ripening as well as particle agglomeration ($\dot{N}_{\mathrm{agg},i}$) due to particle detachment ($\dot{N}_{\mathrm{det},i}$), attachment ($\dot{N}_{\mathrm{att},i}$), and merging ($\dot{N}_{\mathrm{mer},i}$) (Kregar et al., 2020).

Linearization and discretization. For the usage of the non-linear model in the MPC, the non-linear fuel cell model is successively linearized at timestep k with

$$\begin{aligned}
\dot{\mathbf{x}} &= \dot{\mathbf{x}}_k + \underbrace{\frac{\partial \mathbf{f}(\mathbf{x},\mathbf{u},\boldsymbol{\theta})}{\partial \mathbf{x}}|_{\mathbf{x}_k,\mathbf{u}_k,\boldsymbol{\theta}}}_{\mathbf{A}_{c,k}} \Delta\mathbf{x} + \underbrace{\frac{\partial \mathbf{f}(\mathbf{x},\mathbf{u},\boldsymbol{\theta})}{\partial \mathbf{u}}|_{\mathbf{x}_k,\mathbf{u}_k,\boldsymbol{\theta}}}_{\mathbf{B}_{c,k}} \Delta\mathbf{u}\\
\mathbf{y} &= \underbrace{\frac{\partial \mathbf{g}(\mathbf{x},\mathbf{u},\boldsymbol{\theta})}{\partial \mathbf{x}}|_{\mathbf{x}_k,\mathbf{u}_k,\boldsymbol{\theta}}}_{\mathbf{C}_{c,k}} \mathbf{x} + \underbrace{\frac{\partial \mathbf{g}(\mathbf{x},\mathbf{u},\boldsymbol{\theta})}{\partial \mathbf{u}}|_{\mathbf{x}_k,\mathbf{u}_k,\boldsymbol{\theta}}}_{\mathbf{D}_{c,k}=\mathbf{0}} \mathbf{u},
\end{aligned} \tag{12}$$

and discretized according to Böhler et al. (2021). The discrete state-space model is normalized by the respective maximum values for the states, inputs, and outputs to enhance numerical stability, simplify the choice of weighting matrices, and ensure consistent magnitudes in the state matrices.

2.2 Model predictive control algorithm

An MPC formulated in state space (Rawlings et al., 2017) is implemented. The cost function at timestep k

$$\begin{aligned}
J = {} & w_P \sum_{j=k}^{k+N_p} (P_{\mathrm{ref},j|k} - P_{j|k})^2 + \sum_{i=1}^{n_r} w_{r_i} \sum_{j=k}^{k+N_p} r_{i,j|k}^2\\
& + \sum_{i=1}^{n_u} w_{\Delta u_i} \sum_{j=k}^{k+N_c} \Delta u_{i,j|k}^2 + \sum_{i=1}^{n_u} w_{u_i} \sum_{j=k}^{k+N_c} u_{i,j|k}^2\\
& + w_I \left(\sum_{j=1}^{k-1} (P_{\mathrm{ref},j} - P_j) + \sum_{j=k}^{k+N_p} (P_{\mathrm{ref},j|k} - P_{j|k}) \right)^2
\end{aligned} \tag{13}$$

includes costs on the power control error, the rates of degradation, the rate of input change, the absolute value of the inputs, as well as the discrete summation of the power control error weighted by the respective weights w_i. In every timestep k the minimization problem

$$\begin{aligned} \min_{\Delta\mathbf{u}} \quad & J(\Delta\mathbf{x}_{k-1}, \Delta\mathbf{u}, \mathbf{y}_{k-1}) \\ \text{s. t.} \quad & \Delta\mathbf{x}_k = \mathbf{A}_{d,k-1}\Delta\mathbf{x}_{k-1} + \mathbf{B}_{d,k-1}\Delta\mathbf{u}_{k-1}, \\ & \mathbf{y}_k = \mathbf{y}_{k-1} + \mathbf{C}_{d,k-1}\Delta\mathbf{x}_k, \\ & \Delta_{\min}\mathbf{u} \leq \Delta\mathbf{u} \leq \Delta_{\max}\mathbf{u}, \\ & \mathbf{u}_{\min} \leq \mathbf{u} \leq \mathbf{u}_{\max} \end{aligned} \tag{14}$$

is solved as a constrained quadratic programming problem. Not all inputs of the non-linear model are actively controlled - the uncontrolled inputs are kept constant in the prediction step. However, the modular implementation allows for the simple inclusion and exclusion of controlled and uncontrolled inputs. Furthermore, a move-blocking strategy is implemented to consider both the fast dynamics of the internal states and the update rate of the fuel cell system. The sampling time T_s is set to 0.1 s, the inputs are held constant for 1 s and the prediction N_p and control horizon N_c are set to 200 samples.

2.3 Definition of key performance indices

To quantify and compare different weightings in the cost function, three KPIs are defined:

(1) To quantify the fulfillment of the power requirements, the NRMSE $= \frac{1}{P_{\max}}\sqrt{\frac{\sum_{i=1}^{N}(P_{\text{ref},i}-P_i)^2}{N}}$ is used.
(2) The hydrogen usage is considered by the mean hydrogen flow $\bar{H}_2 = \frac{1}{N}\sum_{i=1}^{N}\dot{n}_{\text{H}_2,\text{dry},i}$.
(3) The overall degradation is considered by the ECSA loss %ECSA $= \frac{\text{ECSA}_0 - \text{ECSA}_N}{\text{ECSA}_0}$

These KPIs are intended to give a quick and fair comparison between different design points and weighting matrices in the cost function. Especially when assessing efficiency, further aspects, such as compressor power on the cathode side, overall pressure level, humidification, and cooling power of the fuel cell stack, can and should be considered.

3. RESULTS

3.1 Model parameterization and validation

The submodels (1)-(5) are trained on physical measurement data obtained from a single cell tested on the fuel cell driving load cycle (FC-DLC) (Tsotridis et al., 2015). The data is taken from Zuo et al. (2021), whereby the first FC-DLC (20 minutes) is used as training data, and the subsequent FC-DLC is used as validation data. The non-linear model is simulated with the same inputs as the physical system and the the temperature and voltage responses are compared (Fig. 3). Coefficients of determination of more than 99% for the power and almost 90% for the cell temperature with the validation data are obtained. The parameterization of submodels (6)-(7) is taken from Pandy et al. (2013) and Kregar et al. (2020).

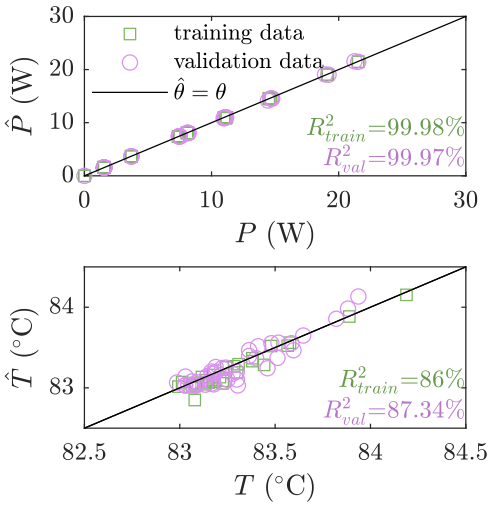

Fig. 3. **Validation of submodels (1)-(5).** The simulated power and cell temperature, denoted by the hat operator, are plotted against the respective measurement data. Similar coefficients of determination are obtained for training and validation data.

3.2 Performance of MPC for different weighting matrices and simulation scenarios

The control algorithm and model are implemented in MATLAB (The MathWorks Inc., 2024) and tested in a simulation setup. The effect of including a physical degradation model in the low-level fuel cell control is shown by comparing three design points for the MPC algorithm (further referred to as the 'MPCs') with different weighting matrices for the rate of degradation. MPC1 does not consider degradation and solely tries to match the required power over time considering the given constraints ($\mathbf{w_r} = \mathbf{0}$). For MPC2 and MPC3, costs for degradation are included, whereby degradation is associated with higher costs for MPC3. Equal weighting for the inputs ($\mathbf{w_u}$), rate of change of the inputs ($\mathbf{w_{\Delta u}}$), the power demand (w_P), and the sum of the power control error (w_I) for all three design points is chosen for fair comparison.

To showcase the impact of actively controlling and optimizing different input variables, the MPCs are tested in two scenarios: (A) only the current and the mole flow into the cathode and anode are actively controlled, and the other inputs are kept constant; (B) additionally, the

Table 1. **KPIs for scenarios A and B and MPC1-3.** Notably, when looking at the KPIs for power and hydrogen consumption, scenarios A and B are very similar. However, by including the control of the inlet dew points (scenario B), significant improvements can be achieved in terms of degradation for MPC2-3.

Scenario	A			B		
MPC	1	2	3	1	2	3
NRMSE (%)	2.18	3.25	4.46	2.18	3.24	4.46
$\bar{H}_2$ (10^2 NLPM)	7.67	9.58	13.14	7.67	9.56	13.04
%ECSA (%)	3.36	2.85	2.46	3.36	2.74	2.12

Increasing performance →

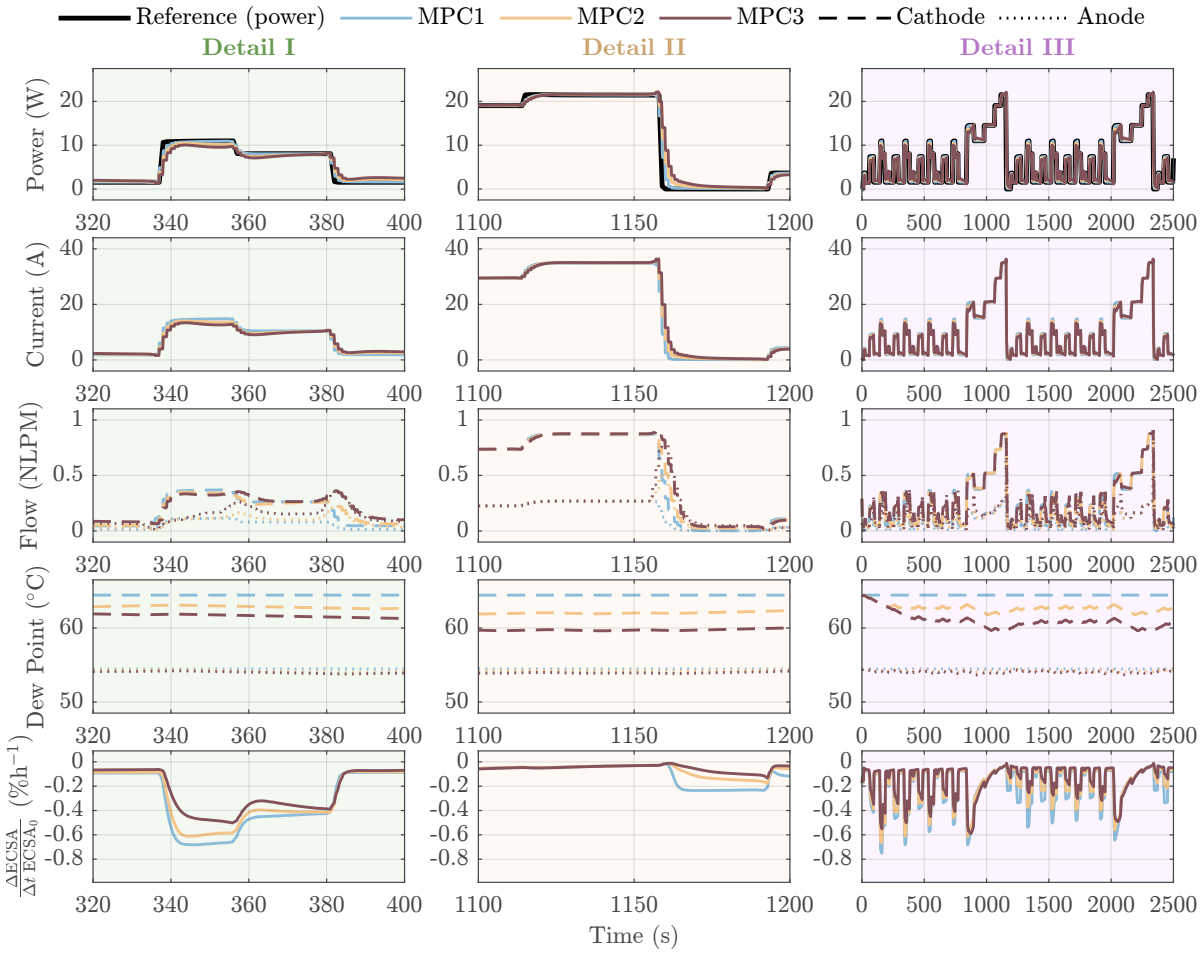

Fig. 4. **Analysis of dynamic behavior of MPCs in scenario B.** For large steps in the power reference (detail I), MPC3 matches the power much slower than the other two MPCs to avoid damaging conditions. For small steps (detail II, first step), the dynamics of the MPCs are almost identical. MPC3 avoids operating the fuel cell at high power as well as in idle operation (detail II). With increasing weights on degradation, the hydrogen flow into the anode increases (middle row), and the humidification of the cathode inlet gas decreases (fourth row). Although degradation can not fully be avoided, the rate of degradation $\frac{\Delta \mathrm{ECSA}}{\Delta t\ \mathrm{ECSA}_0} = \frac{\mathrm{ECSA}_k - \mathrm{ECSA}_{k-1}}{(t_k - t_{k-1})\ \mathrm{ECSA}_0}$ can be reduced (last row) for MPC2-3.

dew point temperatures at the inlet of the electrodes are controlled. Both scenarios have a duration of 20 h of repeating FC-DLC (approx. 60 cycles). Although the FC-DLC does not fully represent real-world driving conditions, it imposes a challenging load profile on the fuel cell covering the whole power operating range. Initialization is equal across all MPCs and scenarios. In the simulation setup, an average real-time factor of around 38.64 is achieved. The scenario includes model linearization, the building of MPC matrices, handling of constraints, solving of a quadratic programming problem, data handling as well as the nonlinear simulation of the fuel cell model used to emulate the physical system behavior.

The KPIs are listed in Table 1. When the objective is to match the required power (MPC1), the best performance in terms of power providing is obtained. By adding degradation phenomena in the cost function, the hydrogen usage and the error on the power demand increase. Notably, by introducing additional degrees of freedom, e.g. the control of the inlet dew point temperatures, degradation can further be decreased while also reducing hydrogen flow. Thus, the reduction of degradation can be achieved by adapting different stressors, which allows for an optimal trade-off between operating costs, efficiency and the longevity of the cell. Moreover, the control strategy effectively balances multiple objectives, optimizing one while minimizing adverse effects on the other. For instance, a 37% reduction in ECSA degradation requires a 70% increase in hydrogen flow (MPC3 compared to MPC1, Scenario B). However, a more moderate hydrogen increase of just 25% can still achieve an 18% reduction in degradation (MPC2 compared to MPC1, Scenario B). This further underscores the advantages of incorporating the nonlinear effects of stressors on degradation into the optimization process. It has to be pointed out that although the NRMSE for MPC3 is much higher than for MPC1, one has to consider that the FC-DLC does impose steep and challenging power steps on the system.

Looking at the dynamic behavior of the MPCs in Fig. 4, the following conclusions can be drawn: In general, higher weightings of degradation lead to slower changes in the current. High power, steep transients, and idle

operation are avoided (Fig. 4, left and middle column). However, for small steps in the power trajectory, all three MPCs have similar fast responses for the power (Fig. 4, middle column), suggesting that operation is adapted dynamically based on how damaging the steps are to the fuel cell system. Furthermore, the suggested control strategy can find a trade-off between different stressors and their impact, i.e., the inlet humidities are not solely minimized, but a trade-off between degradation, performance as well and complex interactions between different stressors are considered (Fig. 4, right column). By including the effects of degradation in low-level control, the rate of degradation can be reduced, and thus, system lifetime is prolonged.

4. CONCLUSION AND OUTLOOK

This paper presented a methodology for a health-conscious MPC approach to manage fuel cell power while minimizing degradation during dynamic operation. The proposed formulation supports real-time implementation, intuitive balancing of power requirements, hydrogen usage, and degradation minimization, and provides valuable insights into the internal processes of the fuel cell. The methodology was evaluated through simulations, where the impact of different weightings was analyzed and compared.

Prospective work will focus on extending the approach to incorporate additional degradation mechanisms, particularly membrane degradation. Further validation will involve testing the algorithm on a more complex, distributed model to better capture real-world conditions. Additionally, advanced state observation techniques will be integrated to ensure practical applicability and robustness in real-world scenarios.

ACKNOWLEDGEMENTS

This work was funded by the Austrian Research Promotion Agency (FFG) by the project AlpeDHues [grant number 884322]. The authors acknowledge the support of this work through the women's promotion program of the Faculty of Mechanical and Industrial Engineering (MWBF) at TU Wien.

REFERENCES

Bartlechner, J., Vrlić, M., Hametner, C., and Jakubek, S. (2024). State-of-Health observer for PEM fuel cells—A novel approach for real-time online analysis. *Int. J. of Hydrogen Energy*, S0360319924008917. doi: 10.1016/j.ijhydene.2024.03.061.

Böhler, L., Ritzberger, D., Hametner, C., and Jakubek, S. (2021). Constrained extended Kalman filter design and application for on-line state estimation of high-order polymer electrolyte membrane fuel cell systems. *Int. J. of Hydrogen Energy*, 46(35), 18604–18614. doi: 10.1016/j.ijhydene.2021.03.014.

Daud, W., Rosli, R., Majlan, E., Hamid, S., Mohamed, R., and Husaini, T. (2017). PEM fuel cell system control: A review. *Renewable Energy*, 113, 620–638. doi: 10.1016/j.renene.2017.06.027.

Ghasemi, R., Sedighi, M., Ghasemi, M., and Sadat Ghazanfarpoor, B. (2023). Design of a Fuzzy Adaptive Voltage Controller for a Nonlinear Polymer Electrolyte Membrane Fuel Cell with an Unknown Dynamical System. *Sustainability*, 15(18), 13609. doi: 10.3390/su151813609.

Kravos, A., Ritzberger, D., Tavčar, G., Hametner, C., Jakubek, S., and Katrašnik, T. (2020). Thermodynamically consistent reduced dimensionality electrochemical model for proton exchange membrane fuel cell performance modelling and control. *J. Power Sources*, 454, 227930. doi:10.1016/j.jpowsour.2020.227930.

Kregar, A., Gatalo, M., Maselj, N., Hodnik, N., and Katrašnik, T. (2021). Temperature dependent model of carbon supported platinum fuel cell catalyst degradation. *J. Power Sources*, 514, 230542. doi: 10.1016/j.jpowsour.2021.230542.

Kregar, A., Tavčar, G., Kravos, A., and Katrašnik, T. (2020). Predictive system-level modeling framework for transient operation and cathode platinum degradation of high temperature proton exchange membrane fuel cells. *Appl. Energy*, 263, 114547. doi: 10.1016/j.apenergy.2020.114547.

Li, Q., Chen, W., Li, Y., Liu, S., and Huang, J. (2012). Energy management strategy for fuel cell/battery/ultracapacitor hybrid vehicle based on fuzzy logic. *Int. J. Electr. Power Energy Syst*, 43(1), 514–525. doi:10.1016/j.ijepes.2012.06.026.

Pandy, A., Yang, Z., Gummalla, M., Atrazhev, V.V., Kuzminyh, N.Y., Sultanov, V.I., and Burlatsky, S. (2013). A Carbon Corrosion Model to Evaluate the Effect of Steady State and Transient Operation of a Polymer Electrolyte Membrane Fuel Cell. *J. Electrochem. Soc.*, 160(9), F972–F979. doi:10.1149/2.036309jes.

Rawlings, J.B., Mayne, D.Q., and Diehl, M. (2017). *Model predictive control: theory, computation, and design*. Nob Hill Publishing, Madison, Wisconsin, 2nd edition edition.

Schneider, P., Sadeler, C., Scherzer, A.C., Zamel, N., and Gerteisen, D. (2019). Fast and Reliable State-of-Health Model of a PEM Cathode Catalyst Layer. *J. Electrochem. Soc.*, 166(4), F322–F333. doi: 10.1149/2.0881904jes.

The MathWorks Inc. (2024). Matlab version: 24.01.0 (R2024a). URL `https://www.mathworks.com`.

Tsotridis, G., Pilenga, A., De Marco, G., and Malkow, T. (2015). *EU harmonised test protocols for PEMFC MEA testing in single cell configuration for automotive applications*. Publications Office, Luxembourg. OCLC: 954062997.

Wallnöfer-Ogris, E., Poimer, F., Köll, R., Macherhammer, M.G., and Trattner, A. (2024). Main degradation mechanisms of polymer electrolyte membrane fuel cell stacks – Mechanisms, influencing factors, consequences, and mitigation strategies. *Int. J. Hydrogen Energy*, 50, 1159–1182. doi:10.1016/j.ijhydene.2023.06.215.

Wu, D., Peng, C., Yin, C., and Tang, H. (2020). Review of System Integration and Control of Proton Exchange Membrane Fuel Cells. *Electrochem. Energ. Rev.*, 3(3), 466–505. doi:10.1007/s41918-020-00068-1.

Zuo, J., Lv, H., Zhou, D., Xue, Q., Jin, L., Zhou, W., Yang, D., and Zhang, C. (2021). Deep learning based prognostic framework towards proton exchange membrane fuel cell for automotive application. *Appl. Energy*, 281, 115937. doi:10.1016/j.apenergy.2020.115937.